ROYAL SOCIETY
OF CHEMISTRY

PAPER

Check for updates

Heating-induced negative temperature coefficient effect in conductive graphene/polymer ternary nanocomposites with a segregated and double-percolated structure†

Shuaiguo Zhao,[a] Dandan Lou,[a] Pengfei Zhan,[a] Guojie Li,[a] Kun Dai, [iD] *[ab]
Jiang Guo,[c] Guoqiang Zheng,[a] Chuntai Liu,[a] Changyu Shen[a] and Zhanhu Guo [iD] *[c]

Electrically conductive polymer composites (CPCs) show considerable promise in thermistors owing to their characteristics of positive temperature coefficient (PTC) effect and negative temperature coefficient (NTC) effect of resistance. In contrast to traditional rigid ceramic thermistors, CPCs are lightweight with good processability, flexibility and variety. However, the development of polymer-based NTC thermistors has been impeded by the polymer volume expansion effect, which usually leads to a PTC effect. Here, we employed a segregated and double-percolated composite microstructure to inhibit the polymer volume expansion effect and flake-like graphene as conductive filler to construct a resistant conductive network by its overlapping contact mode, targeted at developing a favorable NTC material. This strategy was carried out by selectively distributing graphene in a polyamide 6 (PA6) phase between isolated ultrahigh molecular weight polyethylene (UHMWPE) particles. As a result, the graphene/PA6/UHMWPE composites exhibited a relatively linear NTC effect through the whole heating process, a high NTC intensity of 5.1, a wide temperature range of 30–260 °C, good reproducibility as well as high mechanical properties. The underlying mechanism of the NTC effect originates from the morphology evolution from crumpled to stretched morphology, enhanced electron mobility in the crumpled morphology, and the improved conductivity of graphene triggered by increasing the temperature.

1. Introduction

Electrically conductive polymer composites (CPCs) have received considerable attention owing to their multi-functional applications in many engineering and electronic fields.[1–10] A broad range of CPCs are marching toward the aim of developing polymer-based thermistors based on their characteristics of positive temperature coefficient (PTC) effect and negative temperature coefficient (NTC) effect of resistance.[11–14] The PTC effect means an increase in resistance with increasing temperature while the NTC effect is a decrease in resistance with increasing temperature.[13] In contrast to traditional rigid ceramic thermistor, CPCs are lightweight, with good processability, flexibility and variety.

Up to now, CPC-based PTC thermistors have achieved considerable success towards their commercialization in self-regulating heaters, over-current and over-temperature protection.[15–18] However, few polymer-based NTC thermistors with favorable performance have been reported despite their applications in circuit compensation, temperature measurements, and chemical reaction detection.[13,19,20] Specifically, NTC thermistors can be applied in electric circuits and devices where temperature compensation is needed,[19] and can be further applied in lab-on-a-chip techniques for temperature measurements,[21] and in stretchable and wearable electronics for temperature detection, mapping and compensation.[22] The major issue is that most CPCs typically exhibit a PTC effect owing to the detrimental volume expansion effect of the polymer matrix on the conductive network and then an NTC effect in polymer melt due to rearrangement of conductive fillers, instead of the NTC effect alone. This NTC effect can be used for NTC thermistors while the conventional NTC effect of a CPC usually occurs after a PTC effect and, therefore, the CPCs are unsuitable for use as a satisfactory NTC material.

To address this issue, many innovative methods have been proposed. For example, Ansari *et al.* fabricated a poly(vinylidene fluoride) (PVDF)-based NTC material by employing high aspect

[a] School of Materials Science and Engineering, The Key Laboratory of Material Processing and Mold of Ministry of Education, Zhengzhou University, Zhengzhou, Henan 450001, P. R. China. E-mail: kundai@zzu.edu.cn; Tel: +86-371-63887969

[b] State Key Laboratory of Polymer Materials Engineering, Sichuan University, Chengdu, Sichuan 610065, P. R. China

[c] Integrated Composites Laboratory (ICL), Department of Chemical & Biomolecular Engineering, University of Tennessee, Knoxville, TN 37996, USA. E-mail: zguo10@utk.edu

† Electronic supplementary information (ESI) available. See DOI: 10.1039/c7tc02472j

This journal is © The Royal Society of Chemistry 2017

J. Mater. Chem. C, 2017, **5**, 8233–8242 | 8233

ratio graphene, showing high NTC intensity (I_{NTC}, ratio of maximum resistivity to minimum resistivity); however, the ultra-high initial resistivity and nonlinear resistivity response behavior hinder its application.[23] Liu *et al.* reported a slight NTC effect for a high-density polyethylene (HDPE) composite/bundle-like structure multi-walled carbon nanotube (MWCNT) where the contact points between MWCNTs are difficult to separate, which was, however, still followed by an evident PTC effect.[24] Tae *et al.* prepared a poly(*N*-isopropylacrylamide)/carbon nanotubes (CNT) NTC material by phase change-induced increase or decrease in the tunneling barrier, which showed a detection range between 5 and 20 °C and nonlinear responsive behavior.[25] Chu *et al.* demonstrated that with larger aspect ratio of CNTs, a stronger NTC effect was observed in polydimethylsiloxane (PDMS)/ CNTs CPCs due to the increase in contact points between conductive fillers.[26] Yan *et al.* fabricated a flexible PDMS/CNTs NTC thermistor by lithographic filtration method; they found that the I_{NTC} could be tuned from 1.9 at 0% strain to 3 at 50% strain.[22] In general, fabrication of a desired polymer-based NTC thermistor with a high NTC intensity, a linear resistivity response behavior and a wide temperature range remains a tremendous challenge.

Previous research has revealed two valuable points for the fabrication of favorable polymer-based NTC thermistors. The first one is to avoid the separation of contact points between conductive fillers by employing high aspect ratio conductive fillers, such as CNTs. The reason is that wire-like CNTs can generate more overlapping contacts than sphere-like CB particles, leading to a more resistant conductive network.[27,28] Compared to the wire-like conductive network of CNTs, the flake-like overlapping conductive network with more junctions constructed by graphene should make it more difficult to respond to the thermal stimulus,[29–31] and would be a better alternative. The second one is to reduce the destructive volume expansion effect of the polymer matrix to the conductive network. According to Chen *et al.*,[32] a zero-temperature-coefficient effect (ZTC, resistance does not change with increasing the temperature) rather than PTC effect was observed in CB/polypropylene (PP)/polyamide 6 (PA6) composites below 200 °C where CB was selectively distributed in the PA6 phase (double-percolated structure). This ZTC is due to the fact that the PA6 phase effectively protects the CB conductive network from the volume expansion effect of the PP matrix. In addition, the segregated conductive network has also been used to tune the thermal response behaviors of a CPC.[33] The application of a conductive filler with large aspect ratio together with the construction of a segregated and double-percolated conductive structure is therefore believed to be a more probable strategy to develop a novel NTC material, which has not been studied yet.

In the present paper, graphene was selected as the conductive filler and selectively localized in the PA6 phase, and the graphene/ PA6 phase formed continuous conductive layers between isolated ultrahigh molecular weight polyethylene (UHMWPE) particles, generating a fascinating segregated and double-percolated conductive network. The volume ratio of UHMWPE/PA6 was fixed at 70/30 and 1.5 vol% maleic anhydride grafted PE (PEMA) was added to improve the interface adhesion. A novel NTC effect of graphene/PA6/UHMWPE CPCs has been achieved through the

whole heating process from 30 to 260 °C. Consecutive heating–cooling runs were conducted to evaluate the reproducibility. A mechanism considering the stretched morphology and enhanced conductivity of graphene triggered by temperature was proposed to interpret this novel NTC effect. The temperature sensing behaviors of the CB/PA6/UHMWPE and CNTs/PA6/ UHMWPE nanocomposites were also studied for comparison.

2. Experimental

2.1 Materials

UHMWPE (M-II, MFI = 0 g/10 min at 230 °C, 2.16 kg, ρ = 0.94 g cm^{-3}, thermal expansion coefficient α = 1.50 × 10^{-4} mm °C^{-1}) was supplied by Beijing No. 2 Auxiliary Agent Factory. PA6 (M2500I, MFI = 22 g/10 min at 230 °C, 2.16 kg, ρ = 0.90 g cm^{-3}, α = 8.30 × 10^{-4} mm °C^{-1}) was purchased from Guangdong Xinhui Meida Nylon Co., Ltd, China. PEMA, with a grafting ratio of 1%, was obtained from Suzhou Yasai Plastic Co., Ltd, China. Graphene aqueous dispersion with a mass fraction of 0.45 wt% was supplied by Chengdu Organic Chemicals Co. Ltd, China. CNTs with diameter of 10–20 nm and length of 5–20 μm were also provided by Chengdu Organic Chemicals Co. Ltd, Chengdu, China. CB, model VXC-605, was purchased from Cabot Co. Ltd.

2.2 Sample preparation

PEMA pellets were dissolved in xylene at 135 °C with mechanical stirring for 2 h to get a solution with a weight fraction of 10%. After the complete evaporation of xylene, the obtained PEMA bulks were then smashed into powders by a high speed mixer.

For the fabrication of graphene/PA6/UHMWPE composites, a solvent co-coagulation process was employed (Fig. 1). First, PA6 pellets were dissolved in formic acid at 55 °C. The required amount of graphene aqueous dispersion was added into formic acid and then treated under ultrasonication for 10 min to obtain a homogeneous graphene dispersion. The PA6/formic acid and graphene/formic acid were mechanically mixed together. At the same time, UHMWPE and PEMA powders were added into the solution and then ultrasonically treated to achieve a homogeneous mixture. To ensure the simplicity of the schematic, PEMA is not illustrated in Fig. 1. The mixture was flocculated using ethanol, filtered and then dried at 80 °C under vacuum for 24 h. The composites were finally hot-compression molded into films at 240 °C for 10 min under a pressure of 14 MPa. The volume ratio of UHMWPE/PA6 was 70/30, and 1.5 vol% PEMA was added to improve the interface adhesion. For comparison, CB/PA6/UHMWPE, CNTs/PA6/UHMWPE and graphene/PA6 composites were also prepared in the same manner. The dimensions of the samples for the morphological, electrical, mechanical and temperature sensing characterizations were all 40 × 10 × 0.4 mm^3.

2.3 Characterization

For the electrical properties measurements, copper grids were attached to both ends of the sample during the hot-compression process to reduce contact resistance between the sample and the
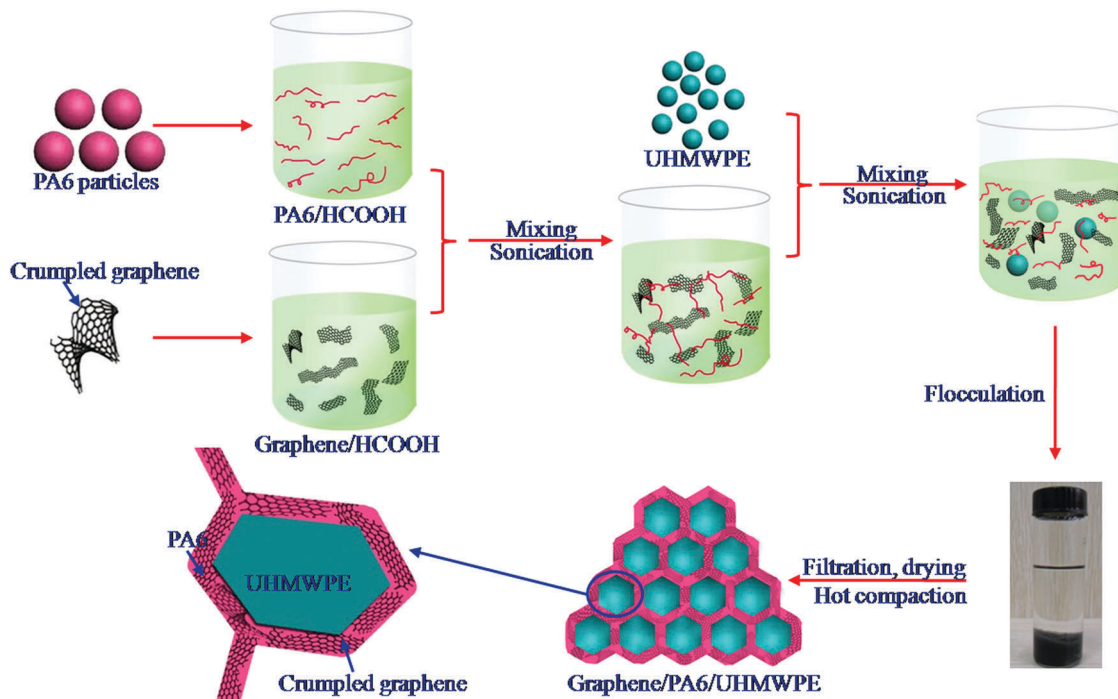
8234 | *J. Mater. Chem. C*, 2017, **5**, 8233–8242

This journal is © The Royal Society of Chemistry 2017

Fig. 1 Schematic for the fabrication of graphene/PA6/UHMWPE composites.

electrode. Volume electrical resistivity lower than 10^6 Ω cm was measured using a four probe method; volume electrical resistivity above 10^6 Ω cm was measured using a high-resistance meter.

The morphology of the composites was observed using a field emission SEM (FESEM, JEOL 7500F, Japan). The specimens were cryogenically fractured after immersion in liquid nitrogen for 30 min and then sputter coated with a thin layer of gold to ensure good conductivity. For optical microscope (OM) observation, the samples were cut into films (15 μm) using a microtome.

The temperature sensing tests were carried out using a temperature-controlled apparatus (Fig. S1, ESI† data). In such a system, the samples were immersed in a silicone oil bath to avoid oxidation. The volume resistivity was recorded *in situ* by a high resistivity meter (Model TH2683, Changzhou Tonghui Electronics Co. Ltd, China). For the temperature resistivity behavior test, all the samples were heated from ambient temperature to 260 °C at 2 °C min^{-1}. Four consecutive heating–cooling runs (HCR, heated to 260 °C at 2 °C min^{-1}, held at 260 °C for 3 min and then cooled at 2 °C min^{-1}) were also performed to check the reproducibility of the temperature resistivity behavior of the graphene/PA6/UHMWPE nanocomposites.

The thermal behavior was examined by differential scanning calorimetry (TA DSC-Q2000) at a heating rate of 2 °C min^{-1} under N$_2$ atmosphere to match the measurement condition of the temperature resistivity behavior. The specimens were also heated from ambient temperature to 260 °C.

The mechanical properties test was carried out using a displacement controlled Suns UTM2203 universal testing machine with a gauge length of 16 mm and a crosshead speed of 50 mm min^{-1}.

3. Results and discussion

3.1 Morphological characteristics

Fig. 2 displays the typical morphology of three conductive fillers, and the optical micrographs and SEM images of the fractured surface of the three composites: graphene/PA6/UHMWPE, CNTs/PA6/UHMWPE and CB/PA6/UHMWPE. In Fig. 2a, graphene exhibits a typical 2D folded plane, which is in good agreement with previous reports.[29–31] The CNTs appear as 1D wire-like strings (Fig. 2b) and CB exists as 0D sphere-like particles (Fig. 2c). For the three composites, a segregated and double-percolated microstructure was successfully constructed, as shown in Fig. 2a'–c'. In the graphene/PA6/UHMWPE nanocomposite (Fig. 2a'), the graphene was selectively dispersed at the PA6 phase, forming a percolated phase; the graphene–PA6 conductive paths surrounded the UHMWPE particles, forming a typical segregated and double-percolated microstructure. The formation of such a unique conductive network originated from the fabrication process. Initially, the graphene and PA6 were pre-mixed and then mechanically stirred with UHMWPE particles; as a result, the graphene/PA6 gradually assembled surrounding the surfaces of UHMWPE particles. Subsequently, during the hot compression, the UHMWPE particles failed to wet the graphene/PA6 phase owing to its high melt viscosity and lack of shear flow. The graphene/PA6 then wrapped up the UHMWPE granules and constructed a segregated microstructure. The selective distribution of graphene in PA6 and the fusion of the graphene/PA6 phase then formed the double-percolated conductive network through the composite. Similar construction of this novel conductive network could also be observed in the CNTs/PA6/UHMWPE and CB/PA6/UHMWPE nanocomposites (Fig. 2b and c).
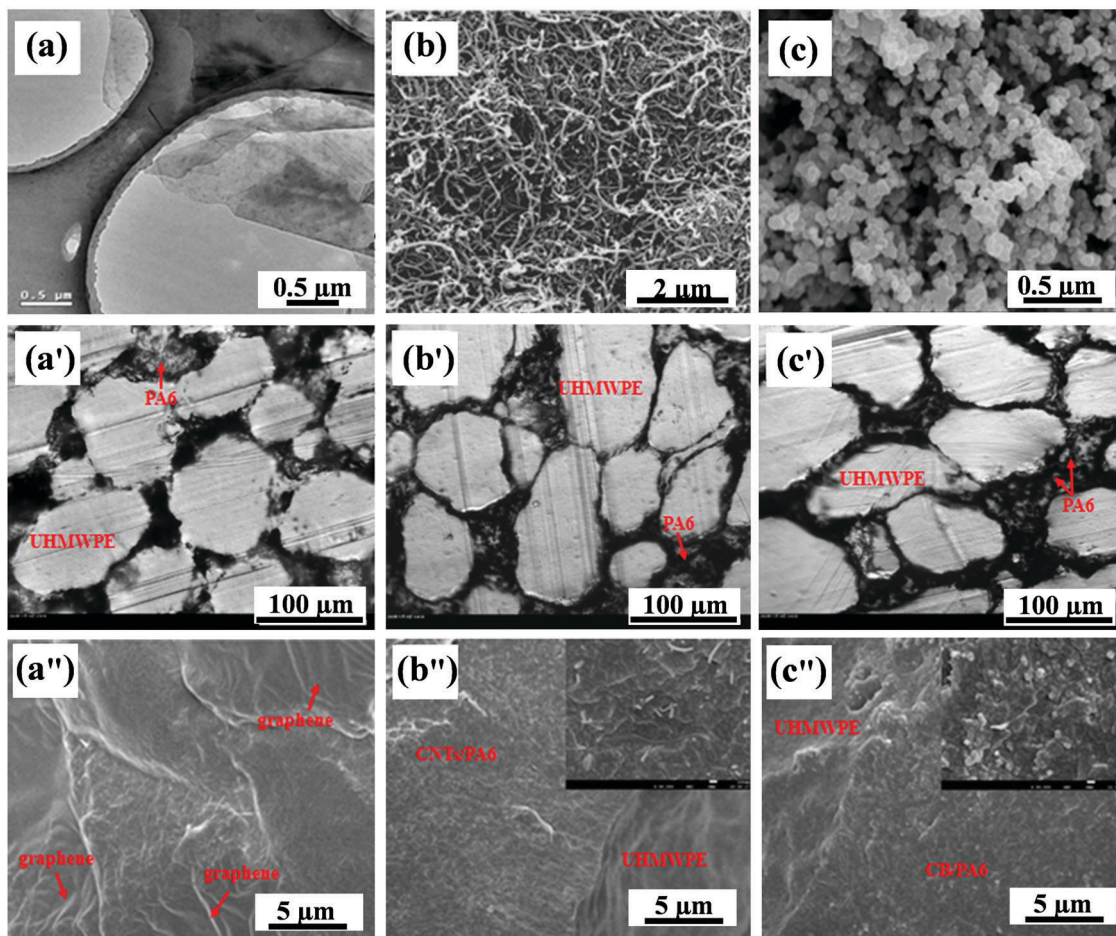
Fig. 2 Morphology characteristics of (a) transmission electron microscopy (TEM) image of graphene and scanning electron microscopy (SEM) images of CNTs (b) and CB (c). Optical and SEM images of the three composites: (a′, a″) graphene/PA6/UHMWPE (0.4 vol% graphene), (b′, b″) CNTs/PA6/UHMWPE (0.24 vol% CNTs) and (c′, c″) CB/PA6/UHMWPE (1.51 vol% CB). The insets in (b″) and (c″) are the CNTs/PA6 and CB/PA6 phase regions with a higher magnification.

In order to investigate the subtle structure of the conductive channels, SEM images were also taken (Fig. 2a″–c″). Obvious crumpled structures in graphene nanosheets were observed in graphene/PA6/UHMWPE (Fig. 2a″). This folded feature of graphene has also been revealed in other literature: the experimental accessible surface area of graphene material is far below the theoretical value of a single graphene sheet, namely 2630 m^2 g^{-1}.[31] Ren et al.[30] reported that the percolation threshold of graphene/UHMWPE (ca. 0.25 wt%) is higher than that of multi-walled MWCNT/UHMWPE (ca. 0.20 wt%). They considered that the graphene sheets were in an overlapping state rather than in plane-to-plane mode and were easier to aggregate than CNTs due to their larger specific surface area, resulting in the high percolation threshold. Results indicate that the folding, crumpling, aggregation and overlapping are easily formed in graphene/polymer composites. With regard to CNTs/PA6/UHMWPE and CB/PA6/UHMWPE (Fig. 2b″ and c″), wire-like CNTs and sphere-like CB particles contacted with each other and formed nice conductive channels in the PA6 domain, respectively.

3.2 Percolation behavior

Fig. 3 displays the volume resistivity as a function of filler content for graphene/PA6/UHMWPE, CNTs/PA6/UHMWPE and CB/PA6/UHMWPE. With increasing filler content, sharp resistivity decreases were observed for the three composites, indicating typical percolation behavior. The percolation thresholds can be further estimated from the three curves by using the classical percolation theory, as shown in eqn (1):[34]

$$\sigma = \sigma_0(\varphi - \varphi_c)^t \tag{1}$$

where φ_c is the percolation threshold, σ is the measured conductivity of the composites, φ is the volume fraction of the filler, and t is the critical exponent. Using eqn (1), the percolation thresholds are estimated to be 0.15 vol% for graphene/PA6/UHMWPE, 0.07 vol% for CNTs/PA6/UHMWPE and 0.59 vol% for CB/PA6/UHMWPE. Here, CNTs/PA6/UHMWPE CPC exhibits the lowest percolation threshold. As discussed in the morphology section, the origin might be from the folding, crumpling, aggregation and overlapping of graphene due to its large specific surface area (Fig. 2a and a″). These factors work together to reduce the utilization ratio of graphene to construct conductive channels. A high percolation threshold was thus experimentally obtained for the graphene/PA6/UHMWPE composites.
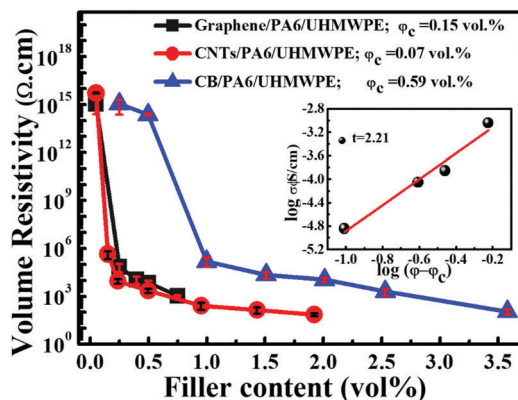
Fig. 3 Volume resistivity as a function of filler content for graphene/PA6/UHMWPE, CNTs/PA6/UHMWPE and CB/PA6/UHMWPE. The inset shows the linear fit of t value for graphene/PA6/UHMWPE.

Fig. 4 DSC curves of the three composites: graphene/PA6/UHMWPE (0.4 vol% graphene), CNTs/PA6/UHMWPE (0.24 vol% CNTs) and CB/UHMWPE (1.51 vol% CB). The heating rate is 2 °C min^{-1}.

In eqn (1), the critical exponent t depends on the dimensionality of the composites and follows a power-law dependence of 1.1–1.3 in a two-dimensional system and 1.6–1.9 in a three-dimensional system. Different from the segregated graphene/UHMWPE composites with a typical two-dimensional conductive network,[35,36] using the data in Fig. 3, t was estimated to be 2.21 in this work, which reveals a nearly three-dimensional conductive network.

In the present paper, the deviation of t possibly originated from the introduction of the conducting graphene/PA6 phase. Primarily, the graphene in the graphene/PA6/UHMWPE composites contacts the crumpled and random structure instead of plane-to-plane mode, leading to more complex conductive networks. In addition, the boundaries between UHMWPE provide relatively large interspaces for graphene to construct a developed conductive network. It is obviously different from single segregated graphene/UHMWPE systems. In a word, the selective distribution of graphene, the novel morphology and the complex conductive network affect the t value significantly, and these factors deviate from the hypothesis of the classical percolation theory, leading to a higher t value.[37]

3.3 Thermal, temperature sensing and mechanical properties

The volume expansion effect, stemming from the melt of polymer crystalline phase, has a great influence on the temperature–resistivity behaviors of CPCs.[12,16,18,38] Here, the thermal properties of these three composites were investigated (Fig. 4). The T_m values and the DSC curves of the composites appear to be similar to each other. A single melting peak around 133 °C was observed in the melt of UHMWPE phase; and two melting peaks at about 217 and 223 °C, corresponding to the melt of γ-form and α-form crystals of PA6, respectively, were also observed obviously.[39]

Fig. 5 displays the temperature–resistivity behaviors of the three composites. Interestingly, in Fig. 5a, the volume resistivity of graphene/PA6/UHMWPE composites decreases rather than increases with increasing temperature, showing an obvious NTC effect. This NTC effect occurs upon the whole heating process, even though the sample is still in the solid state (30–130 °C). This is totally different from the previous reports where the NTC effect occurs only beyond the T_m of the polymer matrix, that is, in the
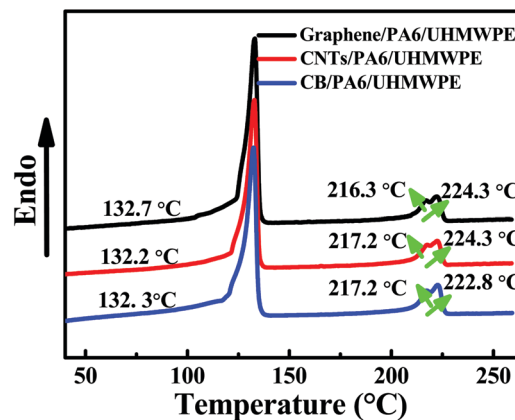
melt state. Although two slight resistivity fluctuations emerge near the T_m of UHMWPE and PA6, respectively, the tendency of the NTC effect could be definitely confirmed. As the temperature increases from 30 to 260 °C, the resistivity of the graphene/PA6/UHMWPE composite decreases from 9.7×10^3 to 1.9×10^3 Ω cm, indicating an I_{NTC} of 5.1. In contrast, in Fig. 5b, the resistivity of the CNTs/PA6/UHMWPE composites exhibits a ZTC effect below 200 °C and then a sharp PTC effect occurs between ca. 200 and 235 °C. The ZTC characteristic between 30 and 200 °C (inset in Fig. 5b) is comparable with the reported ZTC characteristic of bilayer PDMS/CB and PDMS/CNTs between 30 and 200 °C.[13] This ZTC material can be used in heating elements and sensors to precisely control temperature,[13] and in electrostatic discharge protection and electromagnetic interference shielding to ensure stable electrical properties.[40] In Fig. 5c, CB/PA6/UHMWPE composites show a double PTC effect with a weak PTC peak at about 130 °C and a strong PTC peak at about 232 °C, consistent with the volume expansion effect of UHMWPE and PA6.[41,42] Compared to the ZTC effect of CNTs/PA6/UHMWPE, the occurrence of the PTC effect of CB/PA6/UHMWPE is as a result of the vulnerable conductive network constructed by CB particles in non-contact mode.[27,28,43] A clear comparison of the temperature–resistivity behaviors of the three composites is presented in Fig. 5d. Considering the similar microstructure of the conductive network (Fig. 2a′–c′), it can be concluded that graphene takes a highly privileged position in the NTC effect of graphene/PA6/UHMWPE composites.

As discussed in the introduction, it is an extreme challenge to fabricate a semi-crystalline polymer-based NTC material. Most CPCs tend to exhibit a PTC effect due to the polymer volume expansion effect, such as Ni/PVDF,[44] MWCNT/epoxy[45] and CNTs/PP.[46] Despite these challenges, progress has been made by researchers and a summary of the relevant NTC materials is displayed in Fig. 6. Fig. 6 indicates that it is indeed quite difficult to fabricate NTC materials with high I_{NTC} compared to the reported PTC intensity (I_{PTC}, ratio of maximum resistivity to room resistivity) value of PTC materials, namely, up to ca. 10^7 for Ni/PVDF,[44] ca. 3×10^7 for CB/CNTs/UHMWPE/PVDF[45]

This journal is © The Royal Society of Chemistry 2017

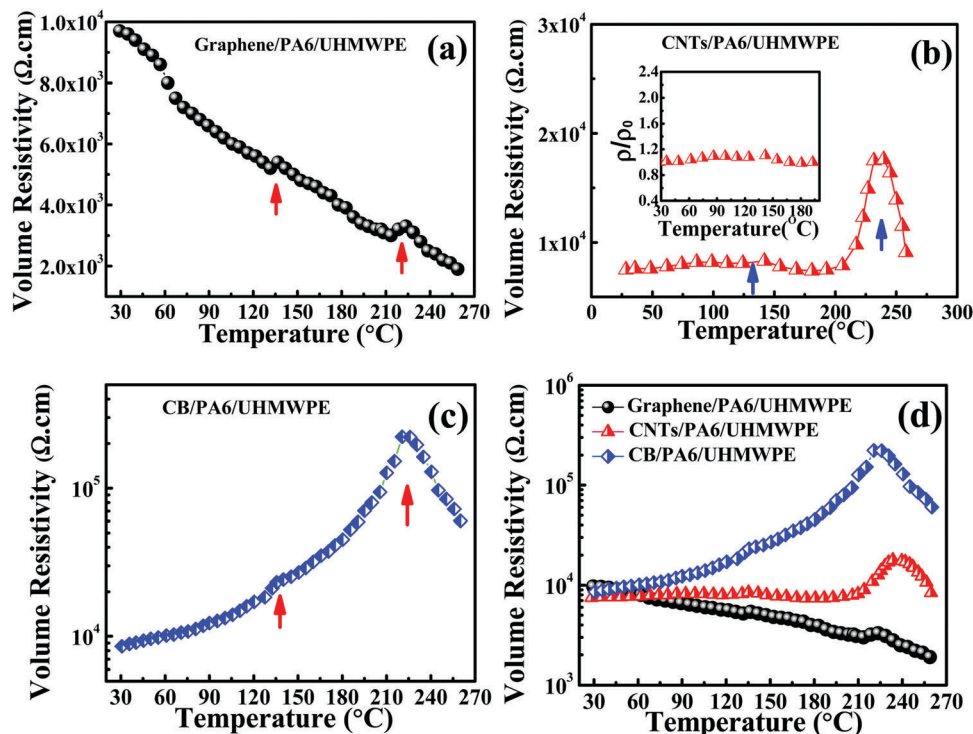J. Mater. Chem. C, 2017, 5, 8233–8242 | 8237

Fig. 5 Temperature dependency of resistivity of (a) graphene/PA6/UHMWPE, (b) CNTs/PA6/UHMWPE and (c) CB/PA6/UHMWPE composites. Representative curves of the three composites are combined in (d) for clear comparison.
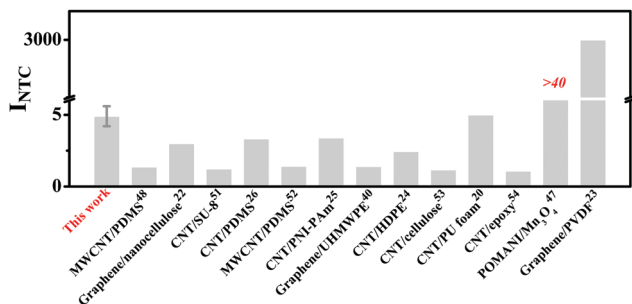

Fig. 6 Summary of some reported I_{NTC} of conductive polymer composites.[20,22–26,40,47,48,50–54] The red value represents a range for I_{NTC}.

and ca. 10^8 for CNTs/PP.[46] The high I_{NTC} in ref. 20, 23 and 47 is possibly due to their large initial resistivity or resistance, namely, 4×10^6 Ω cm for graphene/PVDF,[23] 4×10^7 Ω cm for CNTs/ polyurethane (PU)[20] and above 30 GΩ for poly-o-methyl aniline (POMANI)/Mn$_3$O$_4$,[47] close to the percolation threshold. In this case, the interparticle distance between graphene is quite large and a slight decrease in interparticle distance can result in an obvious reduction in resistivity, that is, a strong NTC effect. This relatively high initial resistivity leads to some issues. For example, very small current would increase the detection requirement and inaccuracy; in addition, to achieve temperature control and compensation, NTC materials with large room resistivity can only make a small change to current, which would mismatch the large change in current caused by PTC material with low room resistivity. On the other hand, both graphene/PVDF[23] and POMANI/ Mn$_3$O$_4$[47] exhibited a non-linear resistivity–temperature response

behavior, making it complex for practical application.[48] In general, the I_{NTC} in this work is much higher than that of many reports and graphene/PA6/UHMWPE also showed a nearly-linear resistivity–temperature response behavior between 30 and 260 °C. There are some other types of NTC material, such as graphene/PDMS and graphene, which, however, are fabricated by the inkjet-printing method and are not similar to the summarized composites.[49,50]

The reproducibility of the NTC effect, which plays a key role in the practical application of NTC materials, was further investigated. Fig. 7 shows the NTC effects of the graphene/ PA6/UHMWPE composites during four HCRs. In each HCR, a resistivity drop upon heating and a resistivity rise upon cooling were detected. Only a slight increase in the resistivity peak and valley was observed, indicating good reproducibility. In the study by Pang et al.,[40] the segregated graphene/UHMWPE composites exhibited a weak NTC effect in the first HCR and a PTC effect in the second HCR, which is attributed to the migration of graphene from the interface region into the UHMWPE granules. The good NTC reproducibility in graphene/ PA6/UHMWPE should be ascribed to the addition of the PA6 phase, which can effectively prevent the migration of graphene. Moreover, the melting point of PA6 (220 °C) is much higher than that of UHMWPE (133 °C), and the solid-state PA6 phase could weaken the volume expansion effect of UHMWPE, leading to a slight resistivity fluctuation below 220 °C.

In order to investigate the influence of the conductive network structure on the NTC effect, the temperature sensing behaviors of CPCs with and without the unique segregated and double-percolated
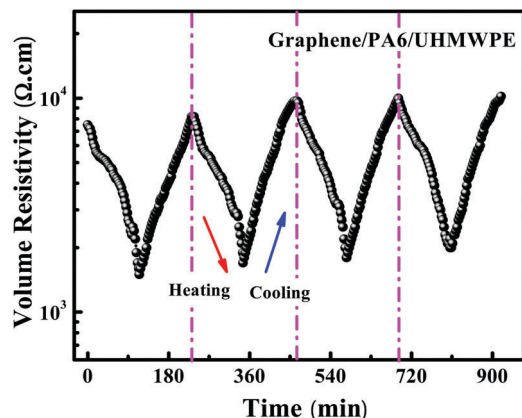
Fig. 7 Volume resistivity as a function of time for the 0.4 vol% graphene/PA6/UHMWPE composites. There are four consecutive HCRs from 30 to 260 °C with a heating and cooling rate of 2 °C min^{-1}.

structure (*i.e.*, graphene/PA6/UHMWPE and graphene/PA6) were studied and compared, as shown in Fig. 8a. The resistance at room temperature is 0.97 MΩ for graphene/PA6/UHMWPE and 1.07 MΩ for graphene/PA6 composites with the same dimensions of 40 × 10 × 0.4 mm.[3] Interestingly, the graphene/PA6 showed a similar NTC effect to that for graphene/PA6/UHMWPE. The difference is that the resistivity of graphene/PA6 decreased quickly below 60 °C and above 224 °C, while graphene/PA6/UHMWPE exhibited a relatively linear behavior. This difference should be attributed to the diminished expansion of PA6 in graphene/PA6/UHMWPE restricted by the neighboring UHMWPE phases. Although the

two composites exhibited similar NTC effects, graphene/PA6 is so brittle that it cannot provide substantial mechanical properties for practical application (Fig. 8b and c). More specifically, in Fig. 8c, the tensile strength and elongation at break of the graphene/PA6/UHMWPE are 29.9 MPa and 34.3% respectively, while they are only 10.3 MPa and 7.73%, respectively, for graphene/PA6.

Based on the above discussions, it can be deduced that the NTC effect is essentially related to the natural features of graphene, and the segregated-double percolated structure provides the composites with excellent electrical and mechanical properties, and a relatively linear resistivity response behavior.

3.4 Theoretical analysis

In general, the composite resistance (R_c) of a CPC above threshold percolation can be approximated as a series of resistors (particle resistance or interparticle resistance) and capacitors (polymer layer between particles) (Fig. 9a and b).[45,55] Due to the applied direct voltage and small value of particle resistance, R_c would be dominated by the interparticle resistance (R_t). Above a critical temperature (*ca.* 25 °C),[28] the polymer volume expansion is evident and the interparticle distance (s) would thus rapidly increase with increasing temperature. Due to the enlarged s, the conduction mechanism is controlled by tunneling effect and R_t is equivalent to tunneling resistance (Fig. 9a and c), described by Balberg's tunneling mechanism:[56]

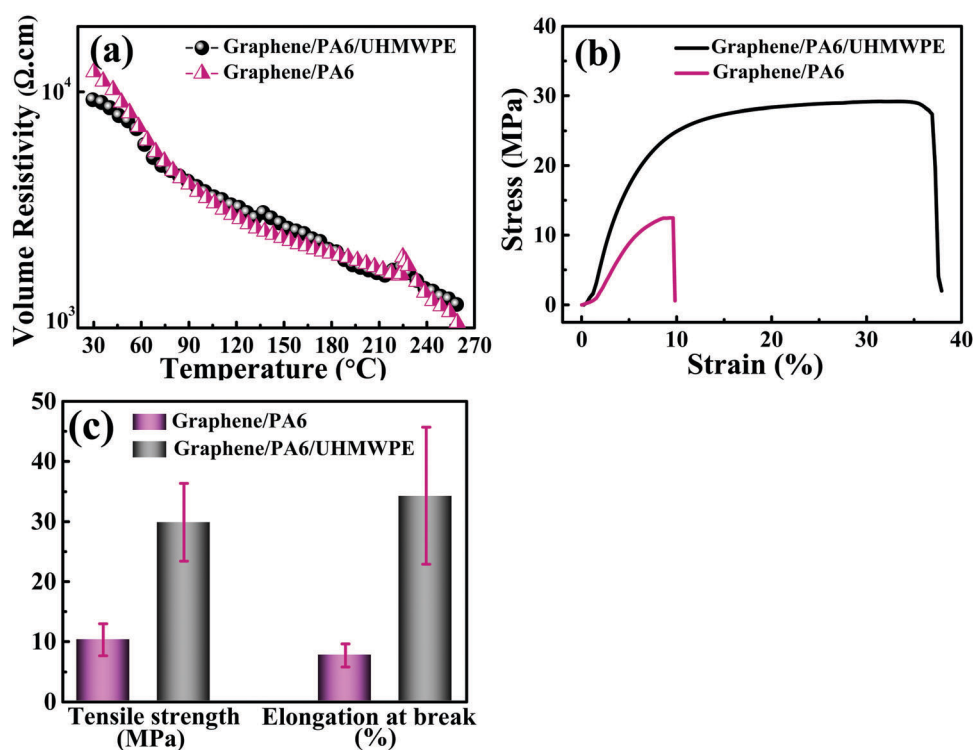$$\sigma_{tun} \propto \exp\left(-\frac{s - 2b}{d}\right) \qquad (2)$$

Fig. 8 Comparison of graphene/PA6/UHMWPE (0.4 vol% graphene) and graphene/PA6 (0.6 vol% graphene) composites: (a) temperature dependency of resistivity, (b) typical stress–strain curves and (c) mechanical properties.

where σ_{tun} means the interparticle tunneling conductivity, d is the tunneling decay parameter and b the radius of the particles. This suggests that R_t would increase exponentially with increasing s because of polymer volume expansion, leading to the common PTC effect.[44–46] Below a critical temperature, the polymer volume expansion is quite trivial and s remains unchanged as the initial small value with increasing temperature. In this case, R_t is equivalent to contact resistance (Fig. 9b) and R_t, would decrease with increasing temperature owing to the increase in the energy and mobility of the electrons, showing an NTC effect.[56–58] This mechanism is termed as variable range hopping (VRH) theory and is expressed by eqn (3) (Fig. 9c):[57,58]

$$\sigma(T) = \sigma_0 \exp(-T_0/T)^{1/(n+1)} \quad (3)$$

Actually, researchers have reported many CPCs with NTC effects below 25 °C.[57–59]

The VRH mechanism was checked for the NTC effect. Fig. 9d shows the curve of $\ln\sigma$ vs. $T^{-1/4}$ where $n = 3$ indicates a 3D conductive network of graphene. Based on the VRH theory,[57] with increasing temperature, the curve should exhibit a constant slope (red line, Fig. 9d), just like the result of pure graphene[60] or a diminishing slope (increased resistivity) due to the detrimental effect of volume expansion.[44] However, an incremental slope (resistivity decreased more quickly) was observed, suggesting that the R_c is governed by contact resistance (Fig. 9b) and, in addition to the VRH mechanism, the only change of the volume expansion effect should also contribute to the decreased resistivity. According to the study by Xiang et al.,[20] external force can reduce the interparticle gap and lead to a decrease in resistivity. In their report, the NTC effect in porous CNTs/PU is caused by the squeeze effect of

expanded CO_2 on CNTs.[20] In our case, however, the thermal expansion coefficient of PA6 (8.30×10^{-4} mm °C^{-1}) is larger than that of UHMWPE (1.50×10^{-4} mm °C^{-1}) and therefore polymer volume expansion could not generate an evident squeeze effect. Otherwise, the resistivity of CB/PA6/UHMWPE and CNTs/PA6/UHMWPE would also decrease.

Except for the squeeze effect, the volume expansion may reduce the interparticle gap or increase contact junctions by composite deformation. Wichmann et al. demonstrated that the MWCNT–MWCNT gap can be reduced by tensile load.[43] The underling mechanism is that under composite deformation by applied strain, MWCNT–MWCNT gap can reduce even though their geometric centers are separated. This is due to the orientation and entanglement effect of CNTs and is only applied for conductive fillers with high aspect ratio.[43] Graphene also has the entanglement effect (not in plan-to-plan mode and crumpled morphology)[20] and both thermally expansion and mechanically stretching of polymer composites are based on the stretch of polymer chains. Therefore, this mechanism can be applied to the NTC effect in this paper.

Based on the above discussions, a schematic for the comprehensive mechanism of the reproducible NTC effect in graphene/PA6/UHMWPE is depicted in Fig. 10. In the heating process, the expanded PA6 polymer chains yield a tension and this deformation can reduce the gap at contact junctions and increase the number of contact junctions by moving graphene or stretching the crumpled graphene. This leads to a reduction in resistivity. Besides, the increased electron mobility based on VRH theory also contributes to the decrease in resistivity. These two factors work together, leading to the novel NTC effect. In the cooling process, polymer chains shrink and the deformation gradually recovers as the
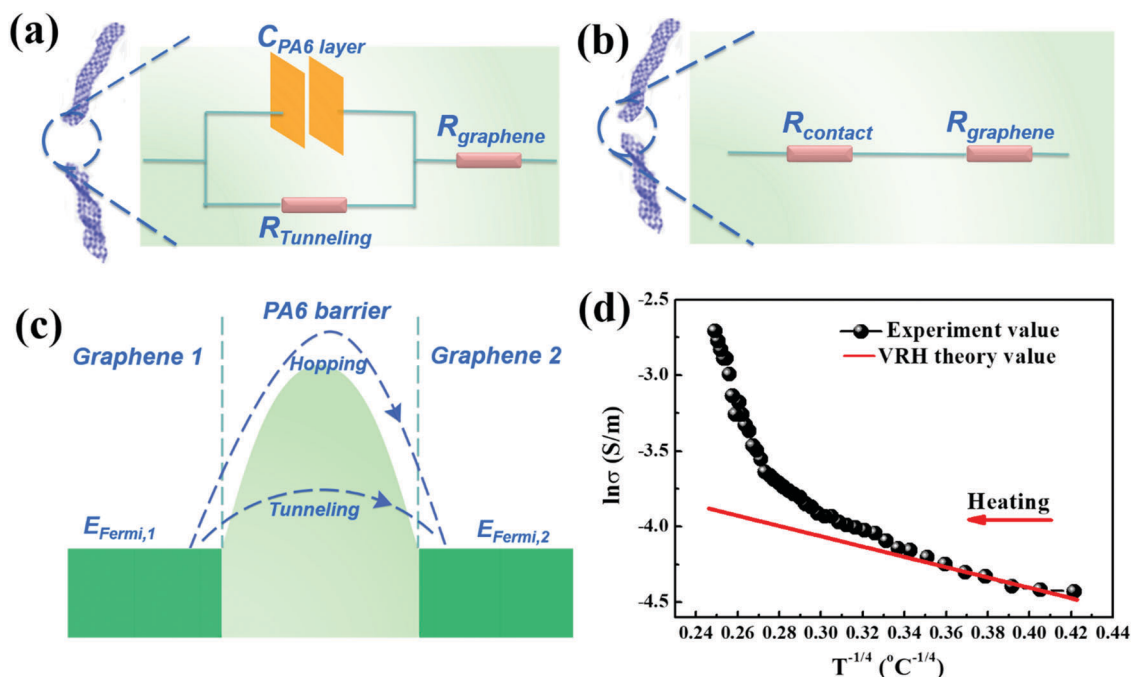

Fig. 9 Schematic of the equivalent circuit of the graphene conductive networks: (a) tunneling resistance and (b) contact resistance; (c) electron transport mode between adjacent conductive particles; and (d) $\ln\sigma$ vs. $T^{-1/4}$ curve for 0.4 vol% graphene/PA6/UHMWPE composites.
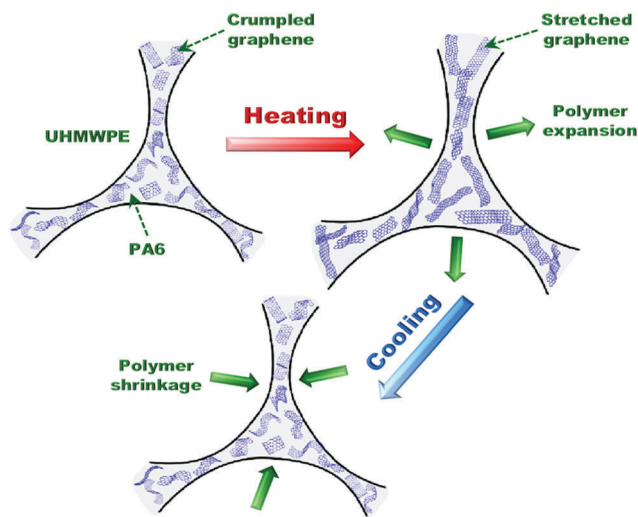
8240 | *J. Mater. Chem. C*, 2017, **5**, 8233–8242

This journal is © The Royal Society of Chemistry 2017

Fig. 10 Schematic illustration of microstructural development for the conductive network in graphene/PA6/UHMWPE composites during heating−cooling runs.

temperature decreases, and finally the conductive network basically restores to its original state. For the unique segregated and double-percolated segregated structure, the PA6 phase ensures not only good reproducibility but also the fairly linear behavior of the NTC effect.

4. Conclusion

A novel NTC material with good reproducibility was fabricated *via* introducing graphene into a UHMWPE-PA6 binary-polymer matrix using a solvent co-coagulation method. The NTC effect has been achieved throughout the whole heating process. For the unique segregated and double-percolated segregated structure, the PA6 phase ensures not only good reproducibility but also the fairly linear behavior of the NTC effect. The temperature resistivity behaviors of CB/PA6/UHMWPE and CNTs/PA6/UHMWPE were also studied for comparison, while no NTC effect was observed through the whole heating. A comprehensive mechanism was proposed to interpret the origin of the NTC effect of graphene/PA6/UHMWPE, that is, the heat-induced morphology transformation of the graphene and the VRH theory work together to transport more electrons through the composites, generating this interesting NTC effect. This method can be used to produce other functional segregated and double-percolated structural nanocomposites with different fillers and polymers for other applications.[61–65] Considering the wide applications of NTC materials in circuit compensation, temperature measurement and control, *etc.*, the novel characteristics of graphene in CPC will be of great importance for the design of multifarious heat-sensitive materials.

Acknowledgements

Notes and references

1 Y. Kim, J. Zhu, B. Yeom, M. Di Prima, X. Su, J. G. Kim, S. J. Yoo, C. Uher and N. A. Kotov, *Nature*, 2013, **500**, 59–63.
2 J. W. Chen, X. H. Cui, Y. T. Zhu, W. Jiang and K. Y. Sui, *Carbon*, 2017, **114**, 441–448.
3 T. Yokota, Y. Inoue, Y. Terakawa, J. Reeder, M. Kaltenbrunner, T. Ware, K. Yang, K. Mabuchi, T. Murakawa, M. Sekino, W. Voit, T. Sekitani and T. Someya, *Proc. Natl. Acad. Sci. U. S. A.*, 2015, **112**, 14533–14538.
4 T. Sekitani, Y. Noguchi, K. Hata, T. Fukushima, T. Aida and T. Someya, *Science*, 2008, **321**, 1468–1472.
5 H. L. Ferrand, S. Bolisetty, A. F. Demirors, R. Libanori, A. R. Studart and R. Mezzenga, *Nat. Commun.*, 2016, **7**, 12078.
6 S. J. Woltornist, D. Varghese, D. Massucci, Z. Cao, A. V. Dobrynin and D. H. Adamson, *Adv. Mater.*, 2017, 1604947.
7 H. Gu, J. Guo, H. Wei, S. Guo, J. Liu, Y. Huang, M. A. Khan, X. Wang, D. P. Young, S. Wei and Z. Guo, *Adv. Mater.*, 2015, **27**, 6277–6282.
8 J. Zhu, S. Wei, M. Alexander, T. Dang, T. Ho and Z. Guo, *Adv. Funct. Mater.*, 2010, **20**, 3076–3084.
9 H. Liu, Y. Li, K. Dai, G. Zheng, C. Liu, C. Shen, X. Yan, J. Guo and Z. Guo, *J. Mater. Chem. C*, 2016, **4**, 157–166.
10 C. Hu, Z. Li, Y. Wang, J. Gao, K. Dai, G. Zheng, C. Liu, C. Shen, H. Song and Z. Guo, *J. Mater. Chem. C*, 2017, **5**, 2318–2328.
11 H. Deng, T. Skipa, E. Bilotti, R. Zhang, D. Lellinger, L. Mezzo, Q. Fu, I. Alig and T. Peijs, *Adv. Funct. Mater.*, 2010, **20**, 1424–1432.
12 S. Bao, G. Liang and S. C. Tjong, *Carbon*, 2011, **49**, 1758–1768.
13 K. Chu, S. C. Lee, S. Lee, D. Kim, C. Moon and S. H. Park, *Nanoscale*, 2015, **7**, 471–478.
14 J. Jeon, H. B. R. Lee and Z. Bao, *Adv. Mater.*, 2013, **25**, 850–855.
15 Y. Zeng, G. Lu, H. Wang, J. Du, Z. Ying and C. Liu, *Sci. Rep.*, 2014, **4**, 6684.
16 A. Rybak, G. Boiteux, F. Melis and G. Seytre, *Compos. Sci. Technol.*, 2010, **70**, 410–416.
17 I. Mironi-Harpaz and M. Narkis, *J. Polym. Sci., Polym. Phys. Ed.*, 2001, **39**, 1415–1428.
18 K. Dai, Z. M. Li and X. B. Xu, *Polymer*, 2008, **49**, 1037–1048.
19 Z. Todorova, N. Dishovsky, R. Dimitrov, F. El-Tantawy, N. Abdel Aal, A. Al-Hajry and M. Bououdina, *Polym. Compos.*, 2008, **29**, 109–118.

This journal is © The Royal Society of Chemistry 2017

J. Mater. Chem. C, 2017, **5**, 8233–8242 | 8241

20 Z. D. Xiang, T. Chen, Z. M. Li and X. C. Bian, *Macromol. Mater. Eng.*, 2009, **294**, 91–95.

21 A. Khosla and B. L. Gray, *Macromol. Symp.*, 2010, **297**, 210–218.

22 C. Yan, J. Wang and P. S. Lee, *ACS Nano*, 2015, **9**, 2130–2137.

23 S. Ansari and E. P. Gianneli, *J. Polym. Sci., Part B: Polym. Phys.*, 2009, **47**, 888–897.

24 F. Liu, X. Zhang, W. Li, J. Cheng, X. Tao, Y. Li and L. Sheng, *Composites, Part A*, 2009, **40**, 1717–1721.

25 P. Tae, C. Zhao, G. E. Fernandes, J. H. Kim and J. Xu, *Nanotechnology*, 2015, **26**, 215705.

26 K. Chu and S. H. Park, *J. Ind. Eng. Chem.*, 2016, **35**, 195–198.

27 H. Nakano, K. Shimizu, S. Takahashi, A. Kono, T. Ougizawa and H. Horibe, *Polymer*, 2012, **53**, 6112–6117.

28 D. Zhu, Y. Bin and M. Matsuo, *J. Polym. Sci., Part B: Polym. Phys.*, 2007, **45**, 1037–1044.

29 C. Yan, J. Wang, W. Kang, M. Cui, X. Wang, C. Y. Foo, K. J. Chee and P. S. Lee, *Adv. Mater.*, 2014, **26**, 2022–2027.

30 P. G. Ren, Y. Y. Di, Q. Zhang, L. Li, H. Pang and Z. M. Li, *Macromol. Mater. Eng.*, 2012, **297**, 437–443.

31 S. Han, D. Wu, S. Li, F. Zhang and X. Feng, *Adv. Mater.*, 2014, **26**, 849–864.

32 G. Chen, B. Yang and S. Guo, *J. Appl. Polym. Sci.*, 2009, **114**, 1848–1855.

33 C. Zhang, C. A. Ma, P. Wang and M. Sumita, *Carbon*, 2005, **43**, 2544–2553.

34 M. Li, C. Gao, H. Hu and Z. Zhao, *Carbon*, 2013, **65**, 371–373.

35 B. Wang, H. Li, L. Li, P. Chen, Z. Wang and Q. Gu, *Compos. Sci. Technol.*, 2013, **89**, 180–185.

36 H. Pang, T. Chen, G. Zhang, B. Zeng and Z. M. Li, *Mater. Lett.*, 2010, **64**, 2226–2229.

37 K. Levon, A. Margolina and A. Z. Patashinsky, *Macromolecules*, 1993, **26**, 4061–4063.

38 H. Deng, T. Skipa, R. Zhang, D. Lellinger, E. Bilotti, I. Alig and T. Peijs, *Polymer*, 2009, **50**, 3747–3754.

39 B. Yin, L. Li, Y. Zhou, L. Gong, M. Yang and B. Xie, *Polymer*, 2013, **54**, 1938–1947.

40 H. Pang, Y. C. Zhang, T. Chen, B. Q. Zeng and Z. M. Li, *Appl. Phys. Lett.*, 2010, **96**, 251907.

41 J. Feng and C. M. Chan, *Polymer*, 2000, **41**, 7279–7282.

42 I. Mironi-Harpaz and M. Narkis, *J. Appl. Polym. Sci.*, 2001, **81**, 104–115.

43 M. H. G. Wichmann, S. T. Buschhorn, J. Gehrmann and K. Schulte, *Phys. Rev. B: Condens. Matter Mater. Phys.*, 2009, **80**, 245437.

44 A. Kono, K. Shimizu, H. Nakano, Y. Goto, Y. Kobayashi, T. Ougizawa and H. Horibe, *Polymer*, 2012, **53**, 1760–1764.

45 J. W. Zha, W. K. Li, R. J. Liao, J. Bai and Z. M. Dang, *J. Mater. Chem. A*, 2013, **1**, 843–851.

46 G. Li, C. Hu, W. Zhai, S. Zhao, G. Zheng, K. Dai, C. Liu and C. Shen, *Mater. Lett.*, 2016, **182**, 314–317.

47 A. Kumar, M. L. Singla, A. Kumar and J. K. Rajput, *Mater. Chem. Phys.*, 2015, **156**, 150–162.

48 P. O. Caffrey and M. C. Gupta, *Appl. Surf. Sci.*, 2014, **314**, 40–45.

49 D. Kong, L. T. Le, Y. Li, J. L. Zunino and W. Lee, *Langmuir*, 2012, **28**, 13467–13472.

50 Y. Gao, W. Shi, W. Wang, Y. Leng and Y. Zhao, *Ind. Eng. Chem. Res.*, 2014, **53**, 16777–16784.

51 J. Duan, W. Wang, B. Zhang, J. Tang, L. Zhao and J. Cui, *Microsyst. Technol.*, 2016, **22**, 2109–2116.

52 S. E. Lee, K. S. Moon and Y. Sohn, *Appl. Phys. Lett.*, 2016, **109**, 021605.

53 H. Qi, B. Schulz, T. Vad, J. Liu, E. Mäder, G. Seide and T. Gries, *ACS Appl. Mater. Interfaces*, 2015, **7**, 22404–22412.

54 H. C. Neitzert, L. Vertuccio and A. Sorrentino, *IEEE Trans. Nanotechnol.*, 2011, **10**, 688–693.

55 Z. Chen, R. Pfattner and Z. Bao, *Adv. Electron. Mater.*, 2017, **3**, 1600397.

56 C. Grimaldi and I. Balberg, *Phys. Rev. Lett.*, 2006, **96**, 066602.

57 M. Aggarwal, S. Khan, M. Husain, T. Ming, M. Tsai, T. Perng and Z. Khan, *Eur. Phys. J. B*, 2007, **60**, 319–324.

58 N. Mott, *J. Non-Cryst. Solids*, 1968, **1**, 1–17.

59 Y. Zhang, C. J. Sheehan, J. Zhai, G. Zou, H. Luo, J. Xiong, Y. T. Zhu and Q. Jia, *Adv. Mater.*, 2010, **22**, 3027–3031.

60 E. P. Boon, L. T. Le and W. Y. Lee, *Carbon*, 2016, **102**, 81–85.

61 (*a*) Z. Sun, L. Zhang, F. Dang, Y. Liu, Z. Fei, Q. Shao, H. Lin, J. Guo, L. Xiang, N. Yerra and Z. Guo, *CrystEngComm*, 2017, **19**, 3288–3298; (*b*) L. Zhang, W. Yu, C. Han, J. Guo, Q. Zhang, H. Xie, Q. Shao, Z. Sun and Z. Guo, *J. Electrochem. Soc.*, 2017, **164**, H651–H656; (*c*) T. Wu, Q. Shao and S. Ge, *RSC Adv.*, 2016, **6**, 58020–58027; (*d*) W. Zhu, S. Ge and Q. Shao, *RSC Adv.*, 2016, **6**, 81736–81743; (*e*) S. Ge, X. Yang, Q. Shao, Q. Liu, T. Wang, L. Wang and X. Wang, *J. Solid State Chem.*, 2013, **200**, 136–142.

62 (*a*) Y. Zheng, Y. Zheng, S. Yang, Z. Guo, T. Zhang, H. Song and Q. Shao, *Green Chem. Lett. Rev.*, 2017, **10**, 202–209; (*b*) Y. Li, X. Wu, J. Song, J. Li, Q. Shao, N. Cao, N. Lu and Z. Guo, *Polymer*, 2017, **124**, 41–47; (*c*) C. Wang, Y. Wu, Y. Li, Q. Shao, X. Yan, C. Han, Z. Wang, Z. Liu and Z. Guo, *Polym. Adv. Technol.*, 2017, DOI: 10.1002/pat.4105; (*d*) W. Yang, X. Wang, J. Li, X. Yan, S. Ge, S. Tadakamalla and Z. Guo, *Polym. Eng. Sci.*, 2017, DOI: 10.1002/pen.24675.

63 J. Guo, H. Song, H. Liu, C. Luo, Y. Ren, T. Ding, M. A. Khan, D. P. Young, X. Liu, X. Zhang, J. Kong and Z. Guo, *J. Mater. Chem. C*, 2017, **5**, 5334–5344.

64 K. Zhang, H. Yu, Y. Shi, Y. Chen, J. Zeng, J. Guo, B. Wang, Z. Guo and M. Wang, *J. Mater. Chem. C*, 2017, **5**, 2807–2817.

65 C. Hu, Z. Li, J. Gao, K. Dai, G. Zheng, C. Liu, C. Shen, H. Song and Z. Guo, *J. Mater. Chem. C*, 2017, **5**, 2318–2328.

8242 | *J. Mater. Chem. C*, 2017, **5**, 8233–8242

This journal is © The Royal Society of Chemistry 2017